Korean J. Chem. Eng., **25**(4), 923-932 (2008)

Evaluation of electrospun nanofiber pore structure parameters

Mohammad Ziabari, Vahid Mottaghitalab, and Akbar Khodaparast Haghi†

University of Guilan, P. O. Box 3756, Rasht, Iran
(*Received 19 August 2007 • accepted 3 October 2007*)

Abstract−Nanofibers produced by electrospinning method are widely used for drug delivery, as tissue scaffolding materials and filtration purposes where specific pore characteristics are required. For continued growth in these areas, it is critical that the nanofibers be properly designed for these applications to prevent failure. Most of the current methods only provide an indirect way of determining pore structure parameters and contain inherent disadvantages. In this study, we developed a novel image analysis method for measuring pore characteristics of electrospun nanofiber webs. Five electrospun webs with different pore characteristics were analyzed by this method. The method is direct, very fast, and presents valuable and comprehensive information regarding pore structure parameters of the webs. Two sets of simulated images were generated to study the effects of web density, fiber diameter and its variations on pore characteristics. The results indicated that web density and fiber diameter significantly influence the pore characteristics, whereas the effect of fiber diameter variations was insignificant.

Key words: Nanofibers, Electrospinning, Image Analysis, Porosity, Pore Size

INTRODUCTION

Fibers with a diameter of around 100 nm are generally classified as *nanofibers*. What makes nanofibers of great interest is their extremely small size. Nanofibers compared to conventional fibers, with higher surface area to volume ratios and smaller pore size, offer an opportunity for use in a wide variety of applications. To date, the most successful method of producing nanofibers is through the process of *electrospinning*. The electrospinning process uses high voltage to create an electric field between a droplet of polymer solution at the tip of a needle and a collector plate. When the electrostatic force overcomes the surface tension of the drop, a charged, continuous jet of polymer solution is ejected. As the solution moves away from the needle and toward the collector, the solvent evaporates and jet rapidly thins and dries. On the surface of the collector, a nonwoven web of randomly oriented solid nanofibers is deposited [1-9]. Fig. 1 illustrates the electrospinning setup.

Material properties such as melting temperature and glass transition temperature as well as structural characteristics of nanofiber webs such as fiber diameter distribution, pore size distribution and fiber orientation distribution determine the physical and mechanical properties of the webs. The surface of electrospun fibers is important when considering end-use applications. For example, the ability to introduce porous surface features of a known size is required if nanoparticles need to be deposited on the surface of the fiber, if drug molecules are to be incorporated for controlled release, as tissue scaffolding materials and for acting as a cradle for enzymes [10]. Besides, filtration performance of nanofibers is strongly related to their pore structure parameters, i.e., percent open area (POA) and pore-opening size distribution (PSD). Hence, the control of the pore of electrospun webs is of prime importance for the nanofibers that are being produced for these purposes. There is no literature available about the pore size and its distribution of electrospun fibers; and in this work, the pore size and its distribution was measured by using an image analysis technique.

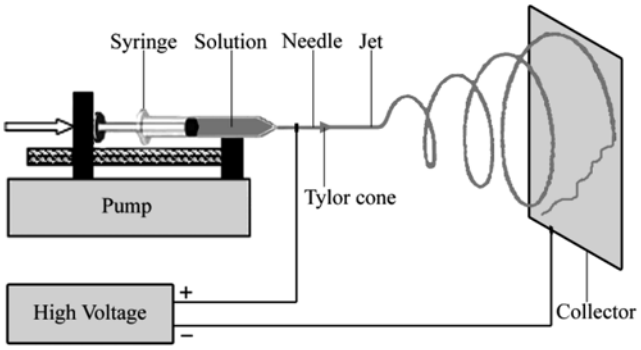

Fig. 1. Electrospinning setup.

Current methods for determining PSD are mostly indirect and contain inherent disadvantages. Recent technological advancements in image analysis offer great potential for a more accurate and direct way of determining the PSD of electrospun webs. Overall, the image analysis method provides a unique and accurate method that can measure pore opening sizes in electrospun nanofiber webs.

METHODOLOGY

The porosity, ε_V, is defined as the percentage of the volume of the voids, V_v, to the total volume (voids plus constituent material), V_t, and is given by

$$\varepsilon_V = \frac{V_v}{V_t} \times 100 \quad (1)$$

Similarly, the percent open area (POA), ε_A, that is defined as the percentage of the open area, A_o, to the total area A_t, is given by

$$\varepsilon_A = \frac{A_o}{A_t} \times 100 \quad (2)$$

†To whom correspondence should be addressed.
E-mail: Haghi@Guilan.ac.ir

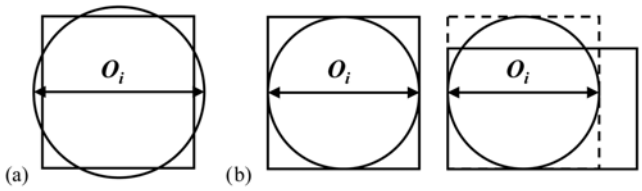

Fig. 2. Equivalent opening size, O_i, based on (a) equivalent area, (b) equivalent size.

Usually porosity is determined for materials with a three-dimensional structure, e.g., relatively thick nonwoven fabrics. Nevertheless, for two-dimensional textiles such as woven fabrics and relatively thin nonwovens it is often assumed that porosity and POA are equal [11].

The size of an individual opening can be defined as the surface area of the opening, although it is mostly indicated with a diameter called equivalent opening size (EOS). EOS is not a single value, for each opening may differ. The common used term in this case is the diameter, O_i, corresponding with the equivalent circular area, A_i, of the opening.

$$O_i=(4A_i/\pi)^{1/2} \quad (3)$$

This diameter is greater than the side dimension of a square opening. A spherical particle with that diameter will never pass the opening (Fig. 2a) and may therefore not be considered as an equivalent dimension or equivalent diameter. This will only be possible if the diameter corresponds with the side of the square area (Fig. 2b). However, not all openings are squares, yet the equivalent square area of openings is used to determine their equivalent dimension because this simplified assumption results in one single opening size from the open area. It is the diameter of a spherical particle that can pass the equivalent square opening, hence the equivalent opening or pore size, O_i, results from

$$O_i=(A_i)^{1/2} \quad (4)$$

From the EOSs, pore size distribution (PSD) and an equivalent diameter for which a certain percentage of the opening have a smaller diameter (O_x, pore opening size that x percent of pores are smaller than that size) may be measured.

The PSD curves can be used to determine the uniformity coefficient, C_u, of the investigated materials. The uniformity coefficient is a measure for the uniformity of the openings and is given by

$$C_u=O_{60}/O_{10} \quad (5)$$

The ratio equals 1 for uniform openings and increases with decreasing uniformity of the openings [11].

Pore characteristic is one of the main tools for evaluating the performance of any nonwoven fabric and for electrospun webs as well. Understanding the link between processing parameters and pore structure parameters will allow for better control over the properties of electrospun fibers. Therefore, there is a need for the design of nanofibers to meet specific application needs. Various techniques may be used to evaluate pore characteristics of porous materials including sieving techniques (dry, wet and hydrodynamic sieving), mercury porosimetry and flow porosimetry (bubble point method) [12,13]. As one goes about selecting a suitable technique for characterization, the associated virtues and pitfalls of each technique should be examined. The most attractive option is a single technique that is non-destructive, yet capable of providing a comprehensive set of data [14].

1. Sieving Methods

In dry sieving, glass bead fractions (from finer to coarser) are sieved through the porous material. In theory, most of the glass beads from the first glass bead fraction should pass. As larger and larger glass bead fractions are sieved, more and more glass beads should become trapped within and on top of the material. The number of pores of a certain size should be reflected by the percentage of glass beads passing through the porous material during each glass bead fraction sieved; however, electrostatic effects between glass beads and between glass beads and the material can affect the results. Glass beads may stick to fibers making the pores effectively smaller and they may also agglomerate to form one large glass bead that is too large to pass through any of the pores. Glass beads may also break from hitting each other and the sides of the container, resulting in smaller particles that can pass through smaller openings.

In hydrodynamic sieving, a glass bead mixture is sieved through a porous material under alternating water flow conditions. The use of glass bead mixtures leads to results that reflect the original glass bead mixture used. Therefore, this method is only useful for evaluating large pore openings such as O_{95}. Another problem occurs when particles of many sizes interact, which likely results in particle blocking and bridge formation. This is especially a problem in hydrodynamic sieving because the larger glass bead particles will settle first when water is drained during the test. When this occurs, fine glass beads which are smaller than the pores are prevented from passing through by the coarser particles.

In wet sieving, a glass bead mixture is sieved through a porous material aided by a water spray. The same basic mechanisms that occur when using the hydrodynamic sieving method also take place with the wet sieving method. Bridge formation is not as pronounced in the wet sieving method as in the hydrodynamic sieving method; however, particle blocking and glass bead agglomeration are more pronounced [12,13].

The sieving tests are very time-consuming. Generally, 2 hours is required to perform a test. The sieving tests are far from providing a complete PSD curve because the accuracy of the tests for pore sizes smaller than 90 μm is questionable [15,16].

2. Mercury Porosimetry

Mercury porosimetry is a well known method often used to study porous materials. This technique is based on the fact that mercury as a non-wetting liquid does not intrude into pore spaces except under applying sufficient pressure. Therefore, a relationship can be found between the size of pores and the pressure applied.

In this method, a porous material is completely surrounded by mercury, and pressure is applied to force the mercury into pores. As mercury pressure increases, the large pores are filled with mercury first. Pore sizes are calculated as the mercury pressure increases. At higher pressures, mercury intrudes into the fine pores and when the pressure reaches a maximum, total open pore volume and porosity are calculated.

The mercury porosimetry thus gives a PSD based on total pore volume and gives no information regarding the number of pores of a porous material. Pore sizes ranging from 0.0018 to 400 μm can

be studied by using mercury porosimetry. Pore sizes smaller than 0.0018 μm are not intruded with mercury, and this is a source of error for porosity and PSD calculations. Furthermore, mercury porosimetry does not account for closed pores, as mercury does not intrude into them. Due to applying high pressures, sample collapse and compression is possible, hence it is not suitable for fragile compressible materials such as nanofiber sheets. Other concerns would include the fact that it is assumed that the pores are cylindrical, which is not the case in reality. After the mercury intrusion test, sample decontamination at specialized facilities is required as the highly toxic mercury is trapped within the pores. Therefore, this dangerous and destructive test can only be performed in well-equipped labs [10,12,13].

3. Flow Porosimetry (Bubble Point Method)

The flow porosimetry is based on the principle that a porous material will only allow a fluid to pass when the pressure applied exceeds the capillary attraction of the fluid in largest pore. In this test, the specimen is saturated with a liquid and continuous air flow is used to remove liquid from the pores. At a critical pressure, the first bubble will come through the largest pore in the wetted specimen. As the pressure increases, the pores are emptied of liquid in order from largest to smallest and the flow rate is measured. PSD, number of pores and porosity can be derived once the flow rate and the applied pressure are known. Flow porosimetry is capable of measuring pore sizes within the range of 0.013-500 μm.

As the air only passes through the pores, characteristics of these pores are measured, while those of closed and blind pores are omitted. Often, 100% total flow is not reached. This is due to porewick evaporation from the pores when the flow rate is too high. Extreme care is required to ensure the air flow does not disrupt the pore structure of the specimen. The flow porosimetry method is also based on the assumption that the pores are cylindrical, which is not the case in reality. Finding a liquid with low surface tension which could cover all the pores, has no interaction with the material and does not cause swelling in material is not always easy and sometimes is impossible [10,12,13].

4. Image Analysis

Because of its convenience in detecting individual pores in a nonwoven image, it seemed to be advantageous to use image analysis techniques for pore measurement. Image analysis was used to measure pore characteristics of woven [15] and nonwoven geotextiles [16]. In the former, successive *erosion* operations with increasing size of *structuring element* were used to count the pore openings larger than a given structuring element. The main purpose of the erosion was to simulate the conditions in the sieving methods. In this method, the voids connected to border of the image which are not complete pores are considered in measurement. Performing opening and then closing operations proceeding pore measurement causes the pore sizes and shapes to deviate from the real ones. The method is suitable for measuring pore sizes of woven geotextiles with fairly uniform pore sizes and shapes and is not appropriate for electrospun nanofiber webs of different pore sizes.

In the latter case, a cross sectional image of nonwoven geotextile was used to calculate the pore structure parameters. A *slicing* algorithm based on a series of morphological operations for determining the mean fiber thickness and the optimal position of the uniform slicing grid was developed. After recognition of the fibers and pores in the slice, the pore opening size distribution of the cross sectional image may be determined. The method is useful for measuring pore characteristics of relatively thick nonwovens and cannot be applied to electrospun nanofiber webs due to extremely small size.

Therefore, there is a need for developing an algorithm suitable for measuring the pore structure parameters in electrospun webs. In response to this need, we have developed a new image analysis based method and presented it in the following.

In this method, a binary image of the web is used as an input. First, voids connected to the image border are identified and cleared by using *morphological reconstruction* [17] where the mask image is the input image and marker image is zero everywhere except along the border. Total area, which is the number of pixels in the image, is measured. Then the pores are labeled and each considered as an object. Here the number of pores may be obtained. In the next step, the number of pixels of each object as the area of that object is measured. Having the area of pores, the porosity and EOS regarding to each pore may be calculated. The data in pixels may then be converted to nm. Finally, a PSD curve is plotted and O_{50}, O_{95} and C_u are determined.

4-1. Real Webs

In order to measure pore characteristics of electrospun nanofibers by image analysis, images of the webs are required. These images called micrographs usually are obtained by scanning electron microscope (SEM), transmission electron microscope (TEM) or atomic force microscope (AFM). The images must be of high quality and taken under appropriate magnifications.

The image analysis method for measuring pore characteristics requires the initial segmentation of the micrographs in order to produce binary images. This is a critical step because the segmentation affects the results dramatically. The typical way of producing a binary image from a grayscale image is by *global thresholding* [17] where a single constant threshold is applied to segment the image. All pixels up to and equal to the threshold belong to object and the remaining belong to the background. One simple way to choose the threshold is picking different thresholds until one is found that produces a good result as judged by the observer. Global thresholding is very sensitive to any inhomogeneities in the gray-level distributions of object and background pixels. In order to eliminate the effect of inhomogeneities, *local thresholding* scheme [17] could be used. In this approach, the image is divided into subimages where the inhomogeneities are negligible. Then optimal thresholds are found for each subimage. A common practice in this case, which is used in this study, is to preprocess the image to compensate for the illumination problems and then apply a global thresholding to the preprocessed image. It can be shown that this process is equivalent to segmenting the image with locally varying thresholds. In order to automatically select the appropriate thresholds, *Otsu's method* [18] is employed. This method chooses the threshold to minimize intraclass variance of the black and white pixels. As it is shown in Fig. 3, global thresholding resulted in some broken fiber segments. This problem was solved by using local thresholding. Note that, since the process is extremely sensitive to noise contained in the image, before the segmentation, a procedure to clean the noise and enhance the contrast of the image is necessary.

4-2. Simulated Webs

In is known that the pore characteristics of nonwoven webs are

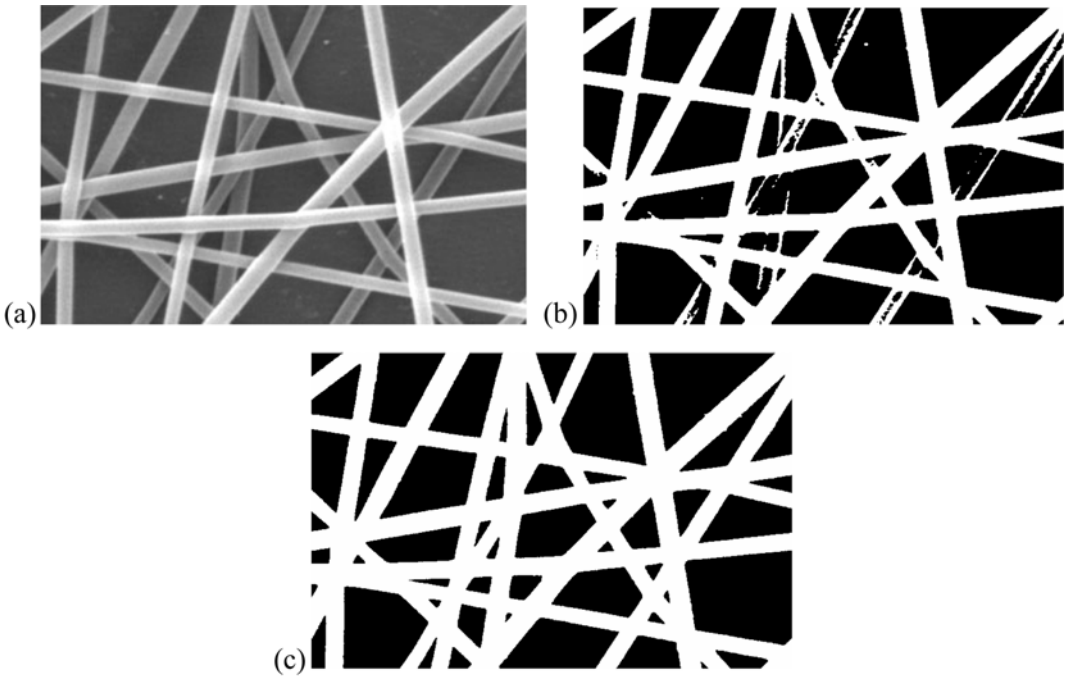

Fig. 3. (a) A real web, (b) Global thresholding, (c) Local thresholding.

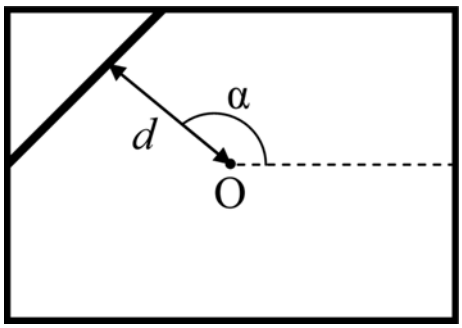

Fig. 4. Procedure for μ-randomness.

influenced by web properties and so are those of electrospun webs. There are no reliable models available for predicting these characteristics as a function of web properties [19]. In order to explore the effects of some parameters on pore characteristics of electrospun nanofibers, simulated webs are generated. These webs are images simulated by straight lines. There are three widely used methods for generating random network of lines: S-randomness, μ-randomness (suitable for generating a web of continuous filaments) and I-randomness (suitable for generating a web of staple fibers). These methods have been described in detail by Abdel-Ghani et al. [20] and Pourdeyhimi et al. [21]. In this study, we used *μ-randomness* procedure for generating simulated images. Under this scheme, a line with a specified thickness is defined by the perpendicular distance d from a fixed reference point O located in the center of the image and the angular position of the perpendicular α. Distance d is limited to the diagonal of the image. Fig. 4 demonstrates this procedure.

One of the most important features of simulation is that it allows several structural characteristics to be taken into consideration with the simulation parameters. These parameters are: web density (controlled as line density), angular density (sampled from a normal or random distribution), distance from the reference point (sampled from a random distribution), line thickness (sampled from a normal distribution) and image size.

Table 1. Electrospinning parameters used for preparing nanofiber webs

No.	Concentration (%)	Spinning distance (cm)	Voltage (KV)	Flow rate (ml/h)
1	8	15	20	0.4
2	12	20	15	0.2
3	8	15	20	0.2
4	8	10	15	0.3
5	10	10	15	0.2

EXPERIMENTAL

Nanofiber webs were obtained from electrospinning of PVA with average molecular weight of 72,000 g/mol (MERCK) at different processing parameters for attaining different pore characteristics. Table 1 summarizes the electrospinning parameters used for preparing the webs. The micrographs of the webs were obtained with a Philips (XL-30) environmental scanning electron microscope (SEM) under magnification of 10,000× after being gold coated. Fig. 5 shows the micrographs of the electrospun webs.

RESULTS AND DISCUSSION

Due to previously mentioned reasons, sieving methods and mercury porosimetry are not applicable for measuring pore structure

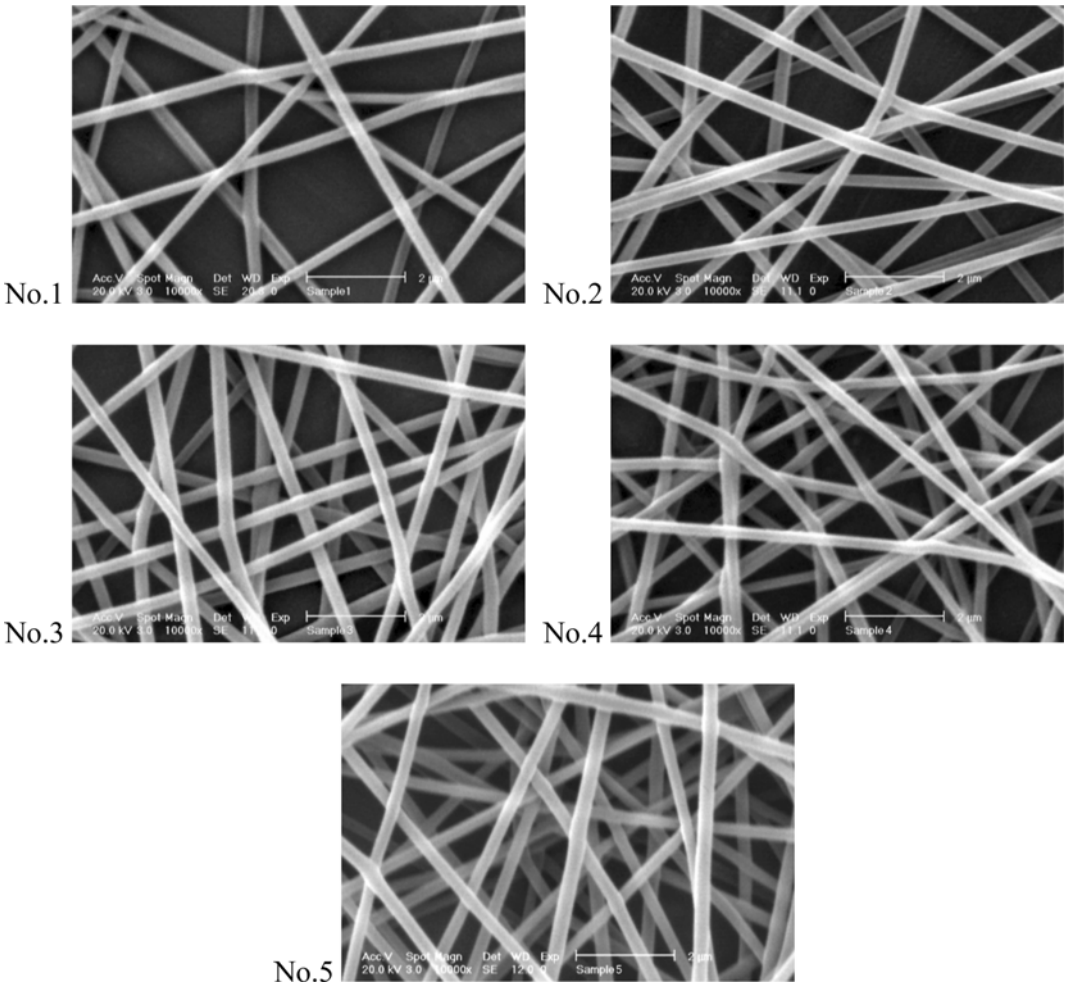

Fig. 5. Micrographs of the electrospun webs.

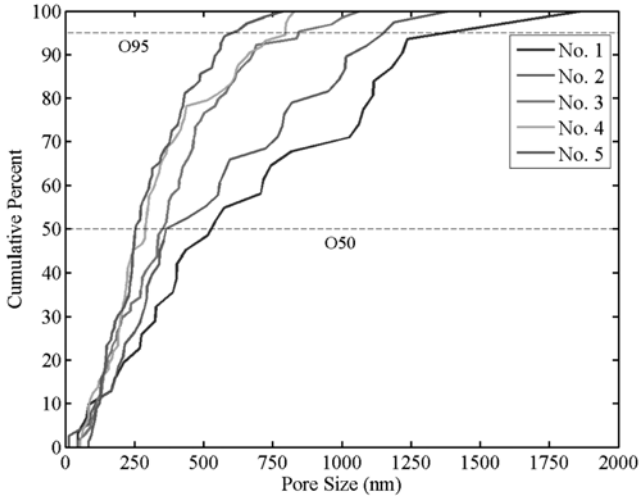

Fig. 6. PSD curves of electrospun webs.

parameters in nano-scale. The only method that seems to be practical is flow porosimetry. However, since in this study the nanofibers were made of PVA, finding an appropriate liquid for the test to be performed is almost impossible because of solubility of PVA in both

Table 2. Pore characteristics of electrospun webs

No.	O_{50}		O_{95}		C_u	Pore no.	Porosity
	pixel	nm	pixel	nm			
1	39.28	513.9	94.56	1237.1	8.43	31	48.64
2	27.87	364.7	87.66	1146.8	5.92	38	34.57
3	26.94	352.5	64.01	837.4	3.73	64	26.71
4	22.09	289.0	60.75	794.8	3.68	73	24.45
5	19.26	252.0	44.03	576.1	2.73	69	15.74

Table 3. Structural characteristics of first set images

No.	Angular range	Line density	Line thickness
1	0-360	20	5
2	0-360	30	5
3	0-360	40	5
4	0-360	20	10
5	0-360	30	10
6	0-360	40	10
7	0-360	20	20
8	0-360	30	20
9	0-360	40	20

organic and inorganic liquids.

As an alternative, image analysis was employed to measure pore structure parameters in electrospun nanofiber webs. PSD curves of the webs, determined by using the image analysis method, are shown in Fig. 6. Pore characteristics of the webs (O_{50}, O_{95}, C_u, number of pores, porosity) measured by this method are presented in Table 2.

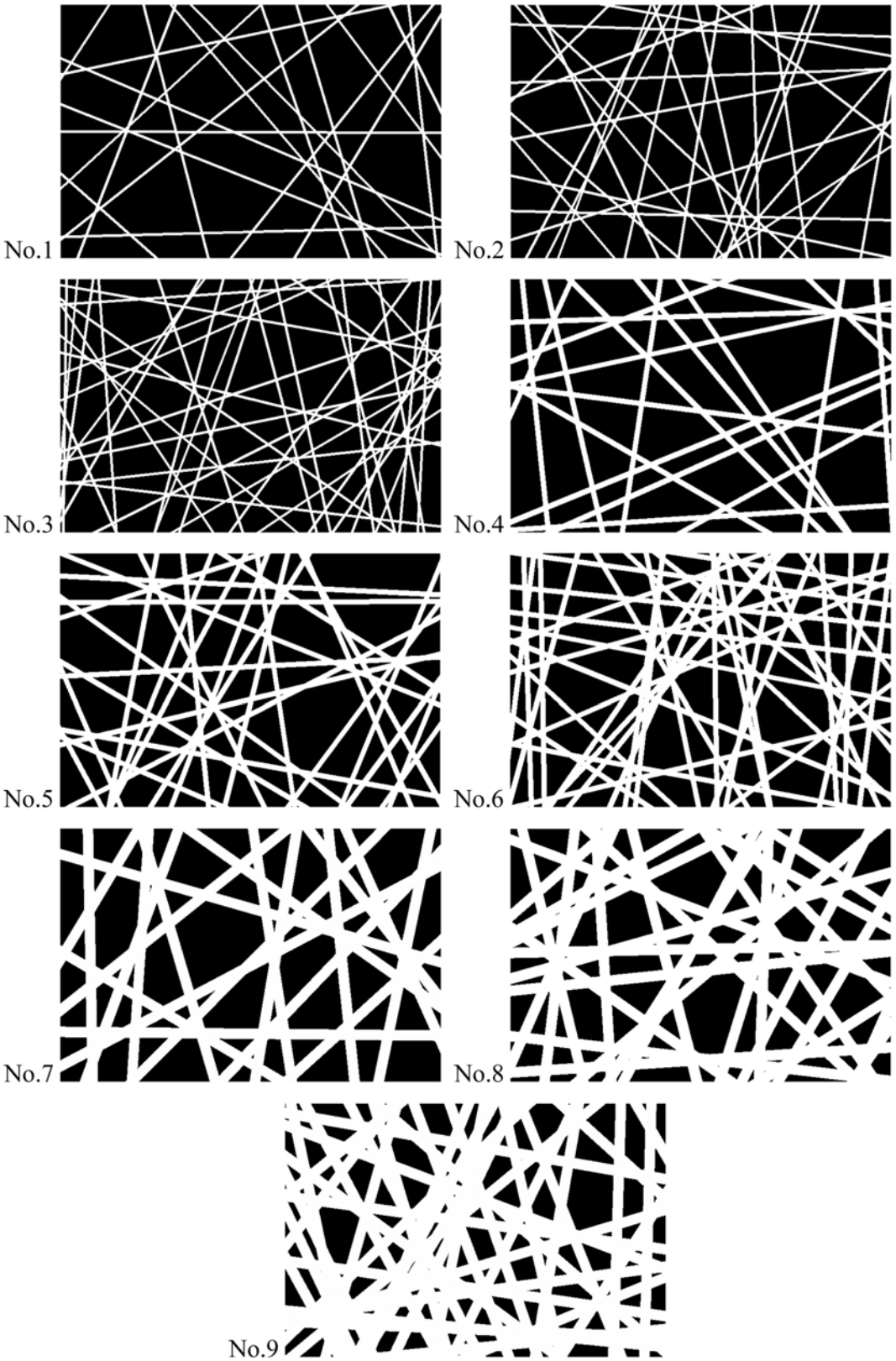

Fig. 7. Simulated images of the first set.

It is seen that decreasing the porosity, O_{50} and O_{95} decrease. C_u also decreases with respect to porosity, that is, increasing the uniformity of the pores. Number of pores has an increasing trend with decreasing the porosity.

The image analysis method presents valuable and comprehensive information regarding pore structure parameters in nanofiber webs. This information may be exploited in preparing the webs with needed pore characteristics to use in filtration, biomedical applications, nanoparticle deposition and other purposes. The advantages of the method are listed below:

1. The method is capable of measuring pore structure parameters in any nanofiber webs with any pore features and it is applicable even when other methods may not be employed.

2. It is very fast. It takes less than a second for an image to be analyzed (using a 3 GHz processor).

3. The method is direct and so simple. Pore characteristics are measured from the area of the pores, which is defined as the number of pixels of the pores.

4. There is no systematic error in measurement (such as assuming pores to be cylindrical in mercury and flow porosimetry and the errors associated with the sieving methods, which were mentioned). Once the segmentation is successful, the pore sizes will be measured accurately. The quality of images affects the segmentation procedure. High-quality images reduce the possibility of poor segmentation and enhance the accuracy of the results.

5. It gives a complete PSD curve.

6. There is no cost involved in the method and minimal technical equipment is needed (SEM for obtaining the micrographs of the samples and a computer for analysis).

7. It has the capability of being used as an on-line quality control technique for large-scale production.

8. The results obtained by image analysis are reproducible.

9. It is not a destructive method. A very small amount of sample is required for measurement.

In an attempt to establish the effects of some structural properties on pore characteristics of electrospun nanofibers, two sets of simulated images with varying properties were generated. The simulated images reveal the degree to which fiber diameter and density affect the pore structure parameters. The first set contained images with the same density varying in fiber diameter and images with the same fiber diameter varying in density. Each image had a constant diameter. The second set contained images with the same density and mean fiber diameter while the standard deviation of fiber diameter varied. The details are given in Table 3 and Table 4. Typi-

Table 4. Structural characteristics of second set images

No.	Angular range	Line density	Line thickness	
			Mean	Std
1	0-360	30	15	0
2	0-360	30	15	4
3	0-360	30	15	8
4	0-360	30	15	10

Table 5. Pore characteristics of the first set of simulated images

No.	O_{50}	O_{95}	C_u	Pore no.	Porosity
1	27.18	100.13	38.38	84	79.91
2	15.52	67.31	22.20	182	71.78
3	13.78	52.32	18.71	308	69.89
4	36.65	94.31	43.71	67	66.10
5	17.89	61.64	22.67	144	53.67
6	12.41	51.60	16.70	245	47.87
7	24.49	86.90	33.11	58	41.05
8	16.31	56.07	21.66	108	32.53
9	13.11	45.38	17.75	126	22.01

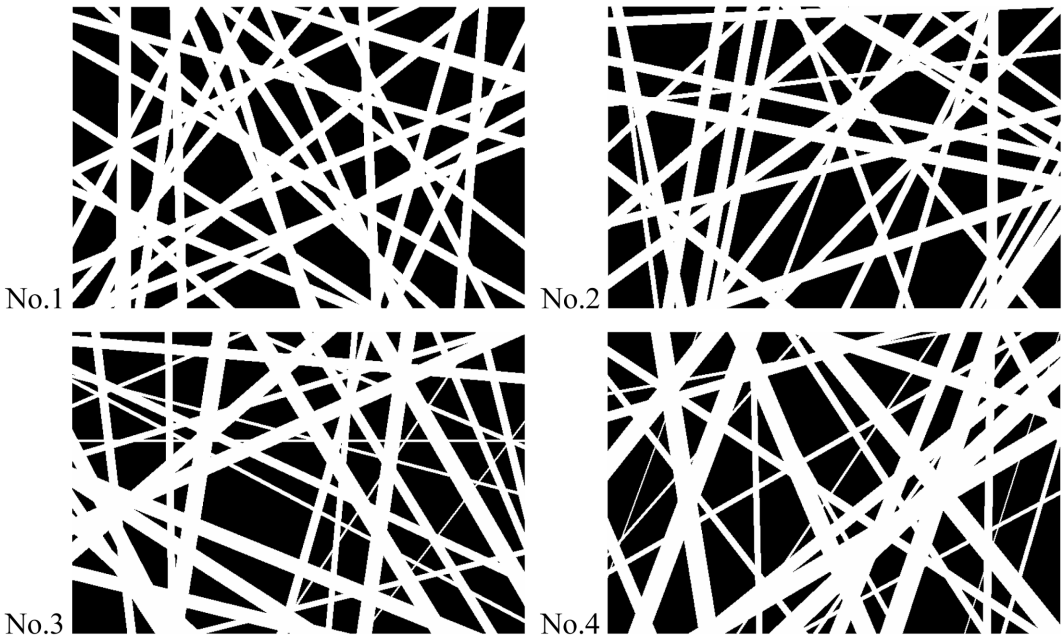

Fig. 8. Simulated images of the second set.

cal images are shown in Fig. 7 and Fig. 8.

Pore structure parameters of the simulated webs were measured by using image analysis method. Table 5 summarizes the pore characteristics of the simulated images in the first set. For the webs with the same density, increasing fiber diameter resulted in a decrease in O_{95}, number of pores and porosity. Assuming the web density to be constant, increasing fiber diameter, the ratio of fibers area to total area (*i.e.* the proportion of white pixels to total pixels in the image) increases, reducing the porosity. It clearly seems that as the fibers

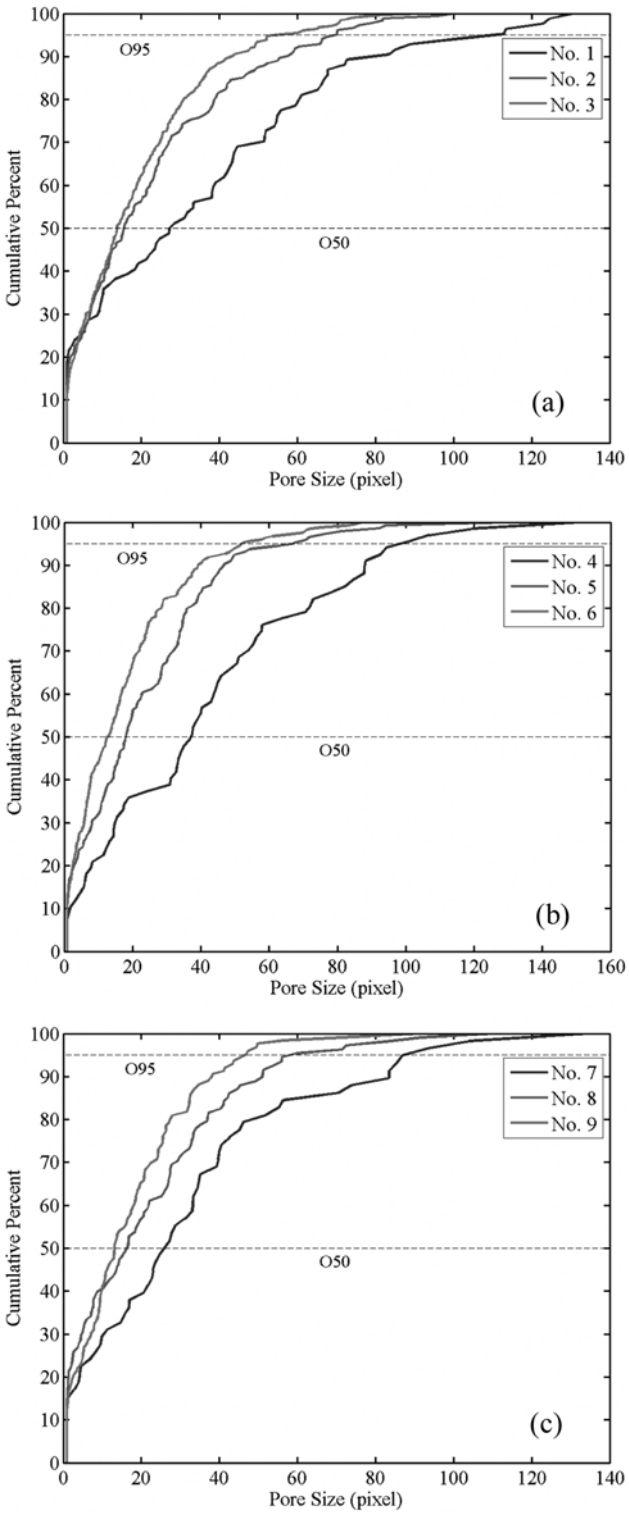

Fig. 9. PSD curves of the first set of simulated images; effect of density, images with the diameter of (a) 5, (b) 10, (c) 20 pixels.

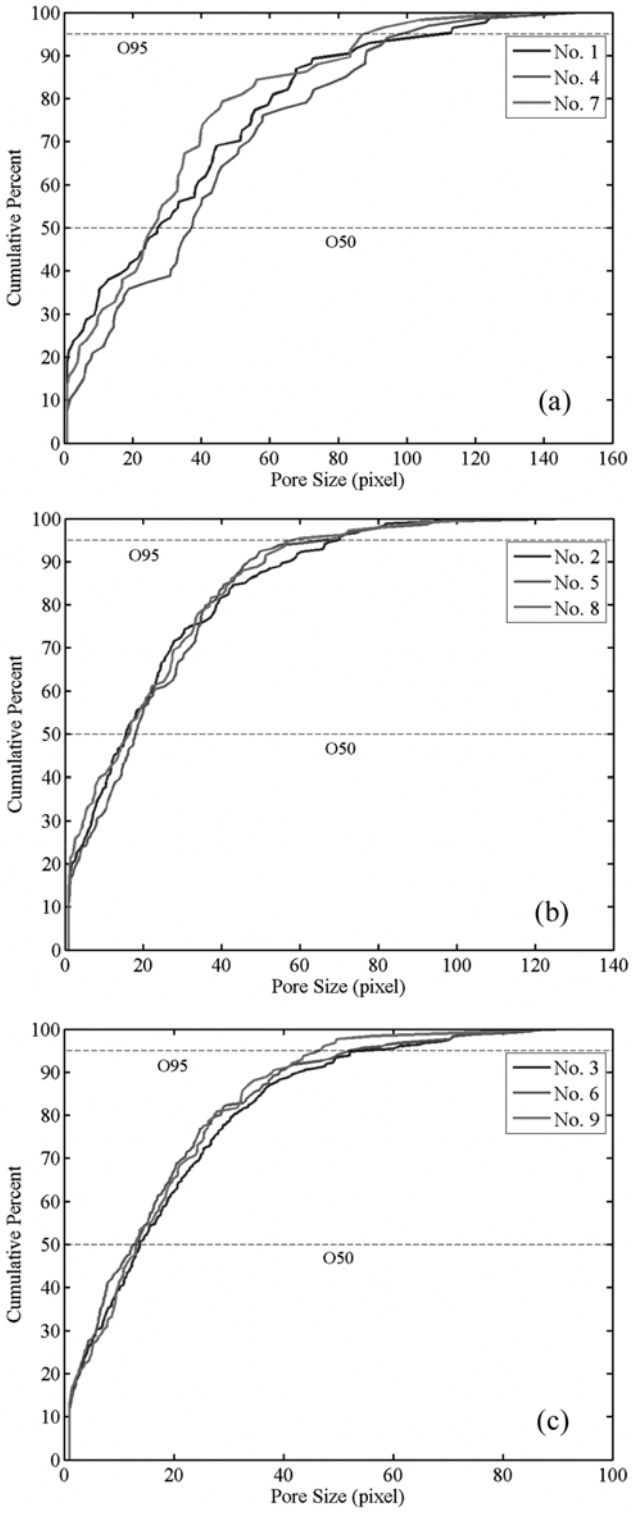

Fig. 10. PSD curves of the first set of simulated images; effect of fiber diameter, images with the density of (a) 20, (b) 30, (c) 40 lines.

get thicker, small pores are covered with the fibers, lowering the number of pores. An increase of fiber diameter at a given web density results in smaller pores; hence O_{95} decreases. No particular trends were observed for O_{50} and C_u. In the case of O_{50}, it is because the effect of fiber diameter is more significant on larger pores while O_{50} is related to mostly small pores and there seem to be other parameters such as the arrangement of the fibers which influence O_{50} more significantly rather than fiber diameter. Since in Eq. (5), O_{10} is in the denominator of the fraction, C_u is very sensitive to variation of O_{10}. This is while O_{10} tends to vary much and almost regardless of fiber diameter (due to aforementioned reason since it is related to very small pores). Hence, other factors such as the way fibers arranged are more dominant and C_u varies regardless of fiber diameter.

Fig. 9 and Fig. 10 show the PSD curves of the simulated images in the first set. As the web density increases, the effects of fiber diameter are less pronounced since the PSD curves of the webs become closer to each other.

For the webs with the same fiber diameter, increasing the density resulted in a decrease in O_{50}, O_{95}, C_u and porosity, whereas the number of pores increased with the density. For the same fiber diameter, total number of fibers and indeed total number of crossovers increases as web density raises, suggesting greater number of pores. It is quite trivial that for a given fiber diameter, the ratio of area of fibers to total area increases as the webs get denser, thus lowering the porosity. Increasing the web density leads to greater number of crossovers. Therefore, large pores are split into several smaller pores. As a result, O_{50} and O_{95} decrease. Furthermore, this fracture of the pores results in less variation of the pore size. Hence, uniformity increases; that is, C_u decreases.

Table 6. Pore characteristics of the second set of simulated images

No.	O_{50}	O_{95}	C_u	Pore no.	Porosity
1	14.18	53.56	18.79	133	35.73
2	13.38	61.66	20.15	136	41.89
3	18.14	59.35	22.07	121	41.03
4	15.59	62.71	20.20	112	37.77

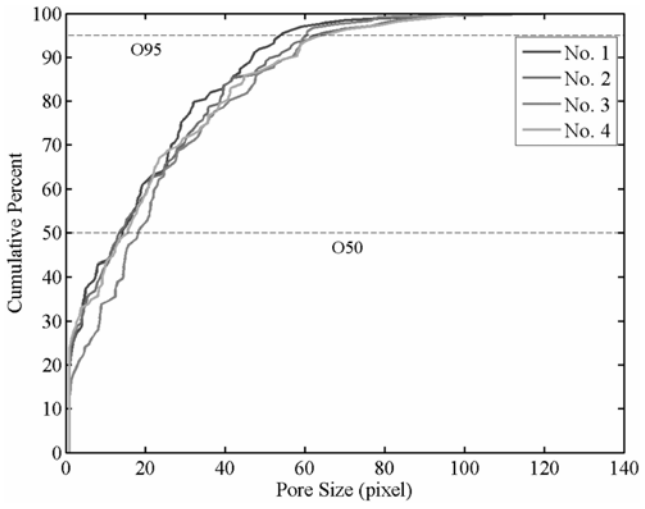

Fig. 11. PSD curves of the second set of simulated images, the effect of fiber diameter variation.

Table 6 summarizes the pore characteristics of the simulated images in the second set. No significant effects for variation of fiber diameter on pore characteristics were observed, suggesting that average fiber diameter is the determining factor, not variation of diameter. Fig. 11 shows the PSD curves of the simulated images in the second set. Holding web density and average fiber diameter constant, the ratio of area of fibers to total area remains the same or fluctuates mostly due to arrangement of the fibers and regardless of variation of fiber diameter. As a result, porosity is not related to variation of fiber diameter. No trends in O_{50} and O_{95} with respect to variation of fiber diameter were observed. This could be attributed to different pore sizes regarding to how thin and thick fibers arrange. The changes in number of pores seem to be independent of variation of fiber diameter as well. It could also be attributed to the arrangement of the fibers.

CONCLUSION

The evaluation of electrospun nanofiber pore structure parameters is necessary as it facilitates the improvement of the design process and its eventual applications. Various techniques have been developed to assess pore characteristics in porous materials. However, most of these methods are indirect, have inherent problems and are not applicable for measuring pore structure parameters of electrospun webs. In this investigation, we have successfully developed an image analysis-based method as a response to this need. The method is simple, comprehensive and so fast and directly measures the pore structure parameters.

The effects of web density, fiber diameter and its variation on pore characteristics of the webs were also explored by using some simulated images. As fiber diameter increased, O_{95}, number of pores and porosity decreased. No particular trends were observed for O_{50} and C_u. Increasing the density resulted in a decrease in O_{50}, O_{95}, C_u and porosity, whereas the number of pores increased with the density. The effects of variation of fiber diameter on pore characteristics were insignificant.

REFERENCES

1. A. K. Haghi and M. Akbari, *Phys. Stat. Sol. (a)*, **204**, 1830 (2007).
2. M. Ziabari, V. Mottaghitalab and A. K. Haghi, *Korean J. Chem. Eng.*, **25**(4), 919 (2008).
3. D. H. Reneker and I. Chun, *Nanotechnology*, **7**, 216 (1996).
4. H. Fong and D. H. Reneker, *Electrospinning and the formation of nanofibers*, In: D. R. Salem, *Structure formation in polymeric Fibers*, Hanser, Cincinnati (2001).
5. Th. Subbiah, G. S. Bhat, R. W. Tock, S. Parameswaran and S. S. Ramkumar, *J. Appl. Polym. Sci.*, **96**, 557 (2005).
6. A. Frenot and I. S. Chronakis, *Curr. Opin. Colloid In.*, **8**, 64 (2003).
7. H. S. Park and Y. O. Park, *Korean J. Chem. Eng.*, **22**, 165 (2005).
8. G. T. Kim, Y. J. Hwang, Y. C. Ahn, H. S. Shin, J. K. Lee and C. M. Sung, *Korean J. Chem. Eng.*, **22**, 147 (2005).
9. G. T. Kim, J. S. Lee, J. H. Shin, Y. C. Ahn, Y. J. Hwang, H. S. Shin, J. K. Lee and C. M. Sung, *Korean J. Chem. Eng.*, **22**, 783 (2005).
10. Ch. L. Casper, J. S. Stephens, N. G. Tassi, D. B. Chase and J. F. Rabolt, *Macromolecules*, **37**, 573 (2004).

11. W. Dierickx, *Geotext. Geomembranes*, **17**, 231 (1999).
12. S. K. Bhatia and J. L. Smith, *Geosynth. Int.*, **3**, 155 (1996).
13. S. K. Bhatia and J. L. Smith, *Geosynth. Int.*, **3**, 301 (1996).
14. S. T. Ho and D. W. Hutmacher, *Biomaterials*, **27**, 1362 (2006).
15. A. H. Aydilek and T. B. Edil, *Geotech. Test. J.*, **27**, 1 (2004).
16. A. H. Aydilek, S. H. Oguz and T. B. Edil, *J. Comput. Civil Eng.*, 280-290 (2002).
17. R. C. Gonzalez and R. E. Woods, *Digital image processing*, 2nd Ed., Prentice Hall, New Jersey (2001).
18. B. Jähne, *Digital image processing*, 5th Ed., Springer, Germany (2002).
19. H. S. Kim and B. Pourdeyhimi, *Intern. Nonwoven J.*, 15-19 (Winter 2000).
20. M. S. Abdel-Ghani and G. A. Davis, *Chem. Eng. Sci.*, **40**, 117 (1985).
21. B. Pourdeyhimi, R. Ramanathan and R. Dent, *Text. Res. J.*, **66**, 713 (1996).